RESEARCH ARTICLE

Development and *In Vivo* Preclinical Imaging of Fluorine-18-Labeled Synaptic Vesicle Protein 2A (SV2A) PET Tracers

Cristian C. Constantinescu[1] Cedric Tresse,[1] MingQiang Zheng,[1] Alexandra Gouasmat,[1] Vincent M Carroll,[1] Laetitia Mistico,[1] David Alagille,[1] Christine M. Sandiego,[1] Caroline Papin,[1] Kenneth Marek,[1] John P. Seibyl,[1] Gilles D. Tamagnan,[1,2] Olivier Barret[1]

[1]Invicro, LLC, 60 Temple St., Suite 8B, New Haven, CT, 06510, USA
[2]Xing Imaging, 760 Temple St., New Haven, CT, 06510, USA

Abstract

Purpose: Synaptic vesicle protein 2A (SV2A) serves as a biomarker of synaptic density and positron emission tomography (PET) imaging of SV2A could provide a tool to assess progression of neurodegenerative diseases. Two tracers have primarily been reported and characterized *in vivo*: [11C]UCB-J and [18F]UCB-H. In early human studies, [11C]UCB-J showed promising results, while its F-18-labeled analogue [18F]UCB-H showed suboptimal specific signal in comparison to [11C]UCB-J. Considering the limited use of [11C]UCB-J to facilities with a cyclotron, having a F-18 variant would facilitate large, multicenter imaging trials. We have screened several F-18 derivatives of UCB-J in non-human primates and identified a promising F-18 PET candidate, [18F]MNI-1126, with additional investigations of the racemate [18F]MNI-1038, affording a signal comparable to [11C]UCB-J.

Procedures: F-18 derivatives of UCB-J and UCB-H were synthesized and administered to non-human primates for microPET imaging. Following screenings, [18F]MNI-1038 (racemate) and [18F]MNI-1126 (R-enantiomer) were identified with the highest signal and favorable kinetics and were selected for further imaging. Kinetic modeling with one- and two-tissue compartmental models, and linear methods were applied to PET data using metabolite-corrected arterial input function. Pre-block scans with levetiracetam (LEV, 10, 30 mg/kg, iv) were performed to determine the tracers' *in vivo* specificity for SV2A. Two whole-body PET studies were performed with [18F]MNI-1038 in one male and one female rhesus, and radiation absorbed dose estimates and effective dose (ED, ICRP-103) were estimated with OLINDA/EXM 2.0.

Results: All compounds screened displayed very good brain penetration, with a plasma-free fraction of ~ 40 %. [18F]MNI-1126 and [18F]MNI-1038 showed uptake and distribution the most consistent with UCB-J, while the other derivatives showed suboptimal results, with similar or lower uptake than [18F]UCB-H. V_T of [18F]MNI-1126 and [18F]MNI-1038 was high in all gray matter regions (within animal averages ~ 30 ml/cm^3) and highly correlated with [11C]UCB-J ($r >$ 0.99). Pre-blocking of [18F]MNI-1126 or [18F]MNI-1038 with LEV showed robust occupancy

Correspondence to: Cristian Constantinescu; *e-mail:* cconstantinescu@invicro.com

across all gray matter regions, similar to that reported with [11C]UCB-J (~ 85 % at 30 mg/kg, ~ 65 % at 10 mg/kg). Using the centrum semiovale as a reference region, BP_{ND} of [18F]MNI-1126 reached values of up to ~ 30 to 40 % higher than those reported for [11C]UCB-J. From whole-body imaging average ED of [18F]MNI-1038 was estimated to be 22.3 μSv/MBq, with tracer being eliminated *via* both urinary and hepatobiliary pathways.

Conclusions: We have identified a F-18-labeled tracer ([18F]MNI-1126) that exhibits comparable *in vivo* characteristics and specificity for SV2A to [11C]UCB-J in non-human primates, which makes [18F]MNI-1126 a promising PET radiotracer for imaging SV2A in human trials.

Key words: SV2A, F-18, PET imaging, Synaptic density, Neurodegenerative disorders, MNI-126

Introduction

Synaptic vesicle proteins 2 (SV2) are a family of 12-transmembrane glycoproteins present in synaptic vesicles of neural and endocrine cells. Among the three known isoforms (SV2A, SV2B, SV2C), SV2A is the most widely expressed and has been the subject of considerable interest in recent years. SV2A proteins are involved in synaptic vesicle exocytosis and neurotransmitter release and can act as a modulator of vesicle fusion [1, 2]. They have been targeted by therapeutic agents for treatment of epilepsy [3–5] due to their brain-specific binding site for levetiracetam, an antiepileptic drug used to treat focal seizures in epilepsy [6, 7], and have been considered as a non-invasive biomarker of synaptic density that can be used for monitoring neurodegenerative diseases [8, 9].

For better insight, more recent efforts have focused on positron emission tomography (PET), a powerful, minimally invasive nuclear imaging technique generally used to visualize and characterize human physiology [10]. Developing PET tracers specific for SV2A offers the potential for a better understanding of the role and function of this target in neurologic conditions such as Alzheimer's disease and epilepsy *in vivo*.

To date, three PET tracers have been reported, [18F]UCB-H, [11C]UCB-A, and [11C]UCB-J [11–14], and while each successfully targeted SV2A, [18F]UCB-H and [11C]UCB-A had less than ideal *in vivo* imaging properties.[11C]UCB-J has been extensively studied and characterized both *in vitro* and *in vivo via* non-human primates and human imaging [6, 9, 15, 16], and it has shown both high specific signal and high *in vivo* affinity.

Fluorine-18 isotope's longer half-life ($t_{1/2} = 110$ min) compared to carbon-11 ($t_{1/2} = 20$ min) allows complex, multi-step syntheses, extended *in vivo* imaging studies, and furthermore from a practical point of view, commercial distribution to satellite clinical PET centers that lack PET isotope production facilities. Thus, the development of a F-18-labeled PET tracer for SV2A with characteristics at least comparable with those of [11C]UCB-J remains a highly pursued goal as it would allow conducting large multi-site clinical trials not limited by the presence of an onsite cyclotron.

Herein, we are reporting the radiosynthesis of several F-18-labeled radioligand derivatives of [11C]UCB-J completed with *in vivo* imaging in non-human primates. We have further selected the best candidate, evaluated it under its racemic ([18F]MNI-1038) and chiral form ((*R*)- [18F]MNI-1126), *via* baseline and blockade studies with levetiracetam (LEV). In addition, we performed whole-body PET scans to assess the biodistribution of [18F]MNI-1038 and provide human dosimetry estimates.

Methods

Radiochemistry

The following procedure describes the radiosynthesis for [18F]MNI-1038, [18F]MNI-1126, and [18F]MNI-1128. In a typical procedure on GE TRACERlab® module, cyclotron target water containing [18F]fluoride was transferred onto and trapped on an ion exchange cartridge. The activity was then eluted with a solution of potassium carbonate and potassium trifluoromethanesulfonate into the reaction vessel and dried under helium at 95 °C for 4 min and the process is repeated twice more with acetonitrile (2 ml total). A solution of precursor (5 mg), Cu(OTf)$_2$ (10 mg), and pyridine (20 μl) in dimethylacetamide (0.7 ml) was added to the reaction vessel and the reaction mixture was heated at 110 °C for 20 min before being cooled at 40 °C and diluted with HPLC eluent and water (1:1, 4 ml). The mixture was transferred into the HPLC loop-loading vial and the entire contents are transferred into the HPLC injector loop for purification. Purification was performed by HPLC using a semi-preparative Waters Xbridge (10 μm, 250 × 10 mm) and eluted with a mixture of acetonitrile/ammonium acetate (20 mM) (30/70, *v/v*) at a flow rate of 4 ml/min. The product fraction was diluted with water and then captured on a tC18 solid-phase extraction cartridge. The cartridge was washed with water and the product was eluted with ethanol where it was further diluted with formulation base (ascorbic acid in saline). The resulting solution was passed through a sterilizing membrane filter into a sterile, filter-vented vial. Detailed synthetic procedures for all tracers are presented in Electronic Supplemental Materials (ESM).

Animals

Adult cynomolgus (*Macaca fascicularis*) and rhesus (*Macaca mulatta*) monkeys housed at the Yale University School of Medicine (New Haven, CT) were used for this study following protocols approved by the Yale University Institutional Animal Care and Use Committee.

PET Study Summary

A single PET scan was performed with [18F]MNI-944 (*rac*-[18F]UCB-J), [18F]MNI-942 ([18F]UCB-H, enantiomer), and [18F]MNI-1080 (*rac*-[18F]UCB-H), in rhesus and cynomolgus monkeys. Four scans were performed with [18F]MNI-1038 (racemate) in one cynomolgus and one rhesus: two baselines and two blocking scans following 30 mg/kg LEV. Four scans were carried out in two rhesus monkeys with [18F]MNI-1126 (R-enantiomer): two baselines and two blocking scans following either 30 mg/kg or 10 mg/kg LEV. LEV was administered as a 5-min iv bolus starting at 15 min before tracer. One rhesus monkey who received both [18F]MNI-1038 and [18F]MNI-1126 was additionally scanned at baseline with [18F]MNI-1128 (S-enantiomer) to facilitate comparison in same animal.

Image Acquisition

Prior to imaging, all animals were induced into anesthesia with ketamine (10 mg/kg) and glycopyrrolate (0.1 mg/kg) at ~2 h before the tracer injection and maintained during the scans with isoflurane (1.5–2 %). PET scans were performed on a Siemens Focus 220 microPET camera (Siemens Healthcare Molecular Imaging, Knoxville, TN, USA). PET images were acquired in list mode over 2–3 h following a 3-min iv bolus administration (173 ± 44 MBq) of a radiotracer. A transmission scan with an external Ge-68 source was performed prior to the emission scans. Images were reconstructed using filtered back projection with standard corrections for random, scatter, and attenuation.

Blood Analysis

Radial artery blood samples were collected over the duration of the scan immediately following tracer injection. Whole blood and plasma samples were counted, and radiometabolites were measured *via* HPLC. Plasma protein binding free fraction (fp) was measured by ultrafiltration. The arterial plasma input function corrected for radiometabolites was used for the modeling of the PET data.

Image Processing

PET images were processed in PMOD 3.8 (PMOD Technologies, Zurich, Switzerland). Images were averaged and aligned onto the monkey's T1-weighted MRI and the transformation applied to the whole PET series and then transformed into a common space *via* spatial normalization of the MRI image to either a rhesus or a cynomolgus monkey template [17, 18]. Volumes of interest (VOIs) were defined by the atlas associated with the templates, except for centrum semiovale, which was defined manually as 3-mm radius circle ROIs placed on three different slices dorsal with respect to the corpus callosum and centered on the cortical white matter. VOIs were applied to the PET series to extract the time–activity curves (TACs). Curves were expressed in SUV (standardized uptake value) by normalizing by the injected dose and animal body weight.

Brain Data Analysis

Time–activity curves were analyzed with one- and two-tissue compartmental models (1T, 2T), which provided estimation of distribution volume, V_T, along with microparameters represented by the kinetic transfer rates. The suitability of either 1T or 2T model to describe the data was determined using the Akaike information criterion (AIC). Regional binding potentials BP_{ND} were estimated as $BP_{ND} = V_T / V_T^{REF} - 1$ using the V_T values in gray matter regions and the centrum semiovale (V_T^{REF}), region with low to negligible SV2A. Logan graphical analysis (LGA) [19] and multilinear analysis (MA1) [20] methods were also explored to derive V_T. Non-displaceable volume of distribution, V_{ND}, was estimated from the (Lassen) occupancy plot [21] at the highest dose of LEV (30 mg/kg), which is described by equation $V_T^{Baseline} - V_T^{Drug} = Occ \times (V_T^{Baseline} - V_{ND})$, where $V_T^{Baseline}$ and V_T^{Drug} are the V_T at baseline and post LEV, respectively. Occ is the global occupancy estimated from the slope of linear regression, and V_{ND} is given by the *x*-intercept. The SV2A regional brain occupancy by LEV was determined as the percent change of BP_{ND}, $Occupancy (\%) = \left(BP_{ND}^{baseline} - BP_{ND}^{drug} \right) / BP_{ND}^{baseline} \times 100$.

[18F]MNI-1038 Dosimetry

Whole-body PET imaging with [18F]MNI-1038 (183 ± 2 MBq, iv) was conducted in two adult cynomolgus monkeys (one 8.2 kg male, one 5.1 kg female) to study the biodistribution and radiation dosimetry of [18F]MNI-1038. The following source organs were used: brain, liver, gallbladder (GB), intestines, urinary bladder (UB), heart content, kidneys, marrow, testes (male), and lungs. Kinetics values (*i.e.*, total number of disintegrations, or residence times) were estimated from dynamic image data. GI tract (ICRP HAT) model [22] with no intestinal reabsorption was used to obtain the kinetics values in different segments of the intestine. GB modeling using 60 % ejection fraction [23] was performed to estimate the GB kinetics value. An UB voiding model assuming a 2-h interval was used to estimate the UB content kinetics value [24]. All kinetics values were

scaled to human based on differences in organ and body weights between the species. The scale factors are provided in the Supplemental Materials. Organ doses and whole-body effective doses were estimated with OLINDA/EXM 2.0 (Hermes Medical Solutions) [25] using ICRP-89 adult male and female models [26]. Effective doses were calculated using biological tissue factors defined in ICRP publications 103 [27] and 60 [28].

Results

Radiochemistry

Our initial efforts focused on the radiosynthesis of [18F]UCB-J by several of recent methodologies. However, the trifluoro moiety proved too challenging to conveniently prepare with fluorine-18, which resulted in only one instance in which the tracer could be prepared through a uronium intermediate and prepared only as a racemate (1, rac-[18F]MNI-944, rac-[18F]UCB-J). The method could be neither scaled nor improved, and the initial [18F]UCB-J goal was abandoned in favor of finding other [18F]UCB-J like compounds that could be readily radiolabeled.

Since the unique trifluoro arrangement proved electronically incompatible to incorporate fluorine-18 efficiently, we sought to alter the original fluorine arrangement by either varying the substitution on the ring or altering the total fluorine content. Synthetic efforts focused on the original UCB-J synthesis but varied to incorporate different benzaldehydes as starting materials as a means to construct the library with a varied fluorine containing arene (data not shown, paper in progress). Initially, the racemic meta difluoro variant (2, MNI-1038) afforded the first hit in the library with the synthesis also amenable to gain access to each enantiomer (3, MNI-1126 and 4, MNI-1128), with all three serving as the basis of our advanced SV2A PET program. To serve as a full comparison of our compounds against known SV2A tracers, [18F]UCB-H (5, [18F]MNI-942) and rac-[18F]UCB-H (6, [18F]MNI-1080) were also prepared (Fig. 1).

Next efforts focused on rendering the lead compounds (2–4) into suitable precursors to incorporate fluorine-18. The presence of both fluorines presiding on an unactivated arene hampered initial synthetic efforts in the type of precursor that would enable this transformation. However, the recent advances in metal-mediated fluorinations; in particular, the Cu/Sn chemistry developed by Scott [29, 30] proved instrumental in enabling the transformation as shown below (Fig. 2), which served as the basis for all radiolabeling studies of [18F]MNI-1038, [18F]MNI-1126, and [18F]MNI-1128.

All the radiolabeling reactions were performed using a GE TRACERlab FX-FN automated synthesis module. Radiolabeling of tin precursors (7) with [18F]fluoride to produce either [18F]MNI-1038, [18F]MNI-1126, or [18F]MNI-1128 (8–10) was achieved using potassium carbonate, potassium triflate, and pyridine in dimethylacetamide and heating at 110 °C for 20 min with the products being purified by semi-preparative HPLC and formulated into a physiological saline/ascorbic acid/ethanol solution. In all cases, the final formulated products were produced in high specific activity (∼ 100–370 GBq/μmol) and radiochemical purity (> 95 %) with the yields averaging between 10 and 20 % decay corrected. Additional Cu and Sn residual analysis of the final product vial by ICP-MS revealed both metals were below the allowable limits specified by ICH guidelines (PDE for Cu: 130 μg/day and PDE for Sn: 640 μg/day with results showing less than 6 μg of each metal) and thus suitable for human injection.

Tracer Metabolism

All tracers tested presented similarly moderate in vivo metabolism. Average fraction of unbound tracer to plasma proteins (i.e., free fraction) of the first six tracer candidates was 40.1 ± 2.3 %. Percentage of unchanged [18F]MNI-1038 (i.e., parent fraction) in cynomolgus and rhesus combined ($n = 4$) was 42.6 ± 9.6 %, 21.2 ± 2.0 %, and 13.6 ± 0.7 %, at 15 min, 60 min, and 120 min, respectively. Average free fraction of [18F]MNI-1038 was 47.1 ± 7.3 %. Parent fraction [18F]MNI-1126 in rhesus ($n = 4$) was 56.0 ± 9.4 %, $27.0 \pm$
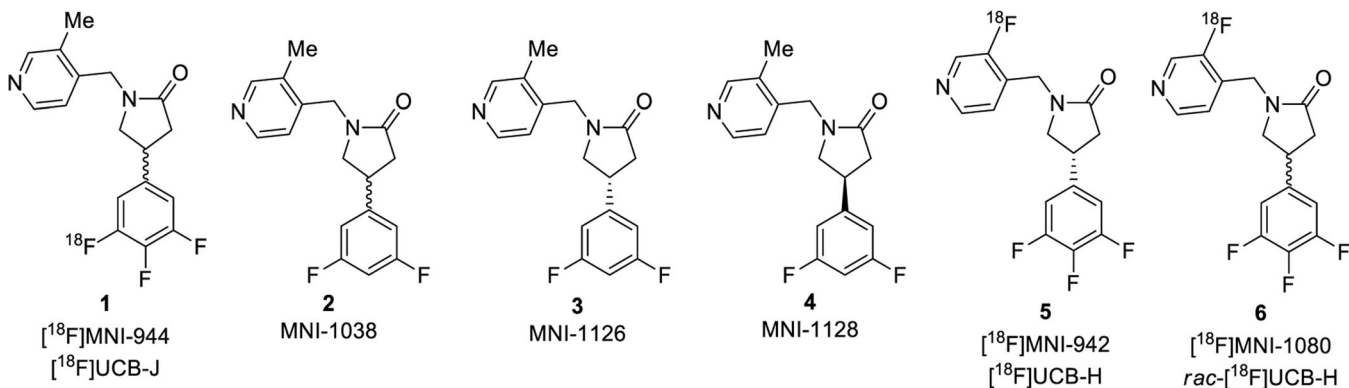

Fig. 1 F-18 radiolabeled derivatives of UCB-J or UCB-H synthesized and tested in vivo.
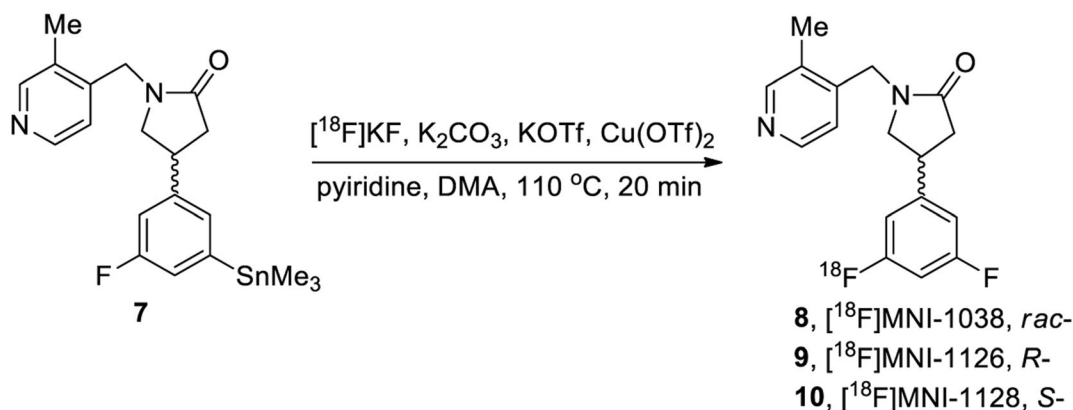
Fig. 2. Radiosynthesis of [^{18}F]MNI-1038 (**8**), [^{18}F]MNI-1126 (**9**), and [^{18}F]MNI-1128 (**10**).

2.1 %, and 20.0 ± 3.0 %, at 15 min, 60 min, and 120 min post injection. Plasma-free fraction of [^{18}F]MNI-1126 was 42.2 ± 2.2 %. No changes in the metabolic profile or free fraction of either tracer attributed to LEV were noted.
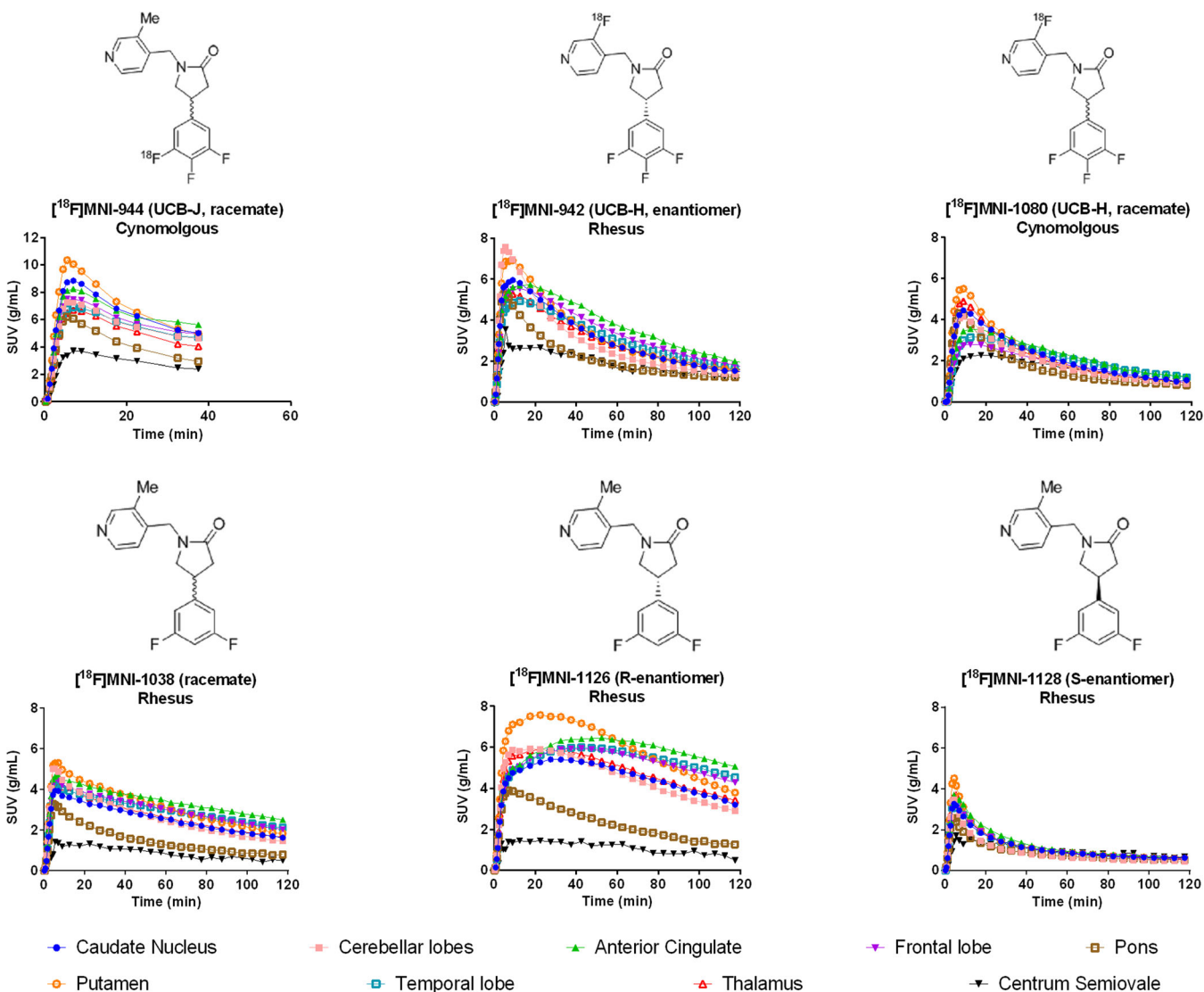

Fig. 3. Summary of F-18-labeled SV2A tracers screening in rhesus and cynomolgus primates, showing time–activity curves (SUV; normalized by primate weight and injected activity) and chemical structure of each tracer.

Brain PET Studies

All tracers screened showed good *in vivo* brain penetration and uptake, with a maximum SUV of 5–8 within 10 min of injection (Fig. 3). [18F]MNI-944(**1**, *rac*-[18F]UCB-J), which was acquired for only 40 min (limited by animal's intolerance of anesthesia) showed uptake and kinetics consistent with literature reports for [11C]UCB-J, but its radiosynthesis could not be reliably reproduced for additional *in vivo* studies. In accordance with literature, [18F]UCB-H (*R*)-isomer (**5**) displayed a higher signal compared to the racemate (**6**), but showed suboptimal signal compared to [18F]UCB-J. LGA (t* = 25 min) with centrum semiovale as reference region applied to our data acquired in rhesus resulted in $BP_{ND} < 1.0$ in all brain regions, similar to BP_{ND} values reported for [18F]UCB-H in human [13].

[18F]MNI-1038 (**8**) and later [18F]MNI-1126 (**9**) showed high uptake and retention, as well as ubiquitous distribution consistent with SV2A in the brain, with highest uptake in the cingulate cortex, cerebral cortex, and putamen, and considerably lower uptake in the white matter of the cerebral centrum semiovale. PET images (averaged over 30–120 min post injection) are shown in Fig. 4a to compare the racemate

[18F]MNI-1038 with [18F]MNI-1126 (*R*-enantiomer) and [18F]MNI-1128 (**10**, *S*-enantiomer). [18F]MNI-1126 and [18F]MNI-1038 demonstrate similar brain distribution with an approximate uptake ratio of 2:1 in favor of [18F]MNI-1126. [18F]MNI-1128 showed very low signal and uniform brain distribution. The corresponding regional time–activity curves (TACs) presented for up to 120 min post injection are compared in Fig. 4b. [18F]MNI-1126 reached peak %ID in the whole brain of up to ~9 %, and peak SUV of 7 to 12, reached at 7 to 50 min post injection (30 ± 12 min). [18F]MNI-1038 reached peak %ID in the whole brain of up to ~9 %, and peak SUV of up to 4 to 6 reached at 6 ± 1 min after injection in rhesus and 18 ± 9 min in cynomolgus. The 1T model produced better (lower AIC) and more reliable (low SE) fits than 2T for [18F]MNI-1126. The 2T model was needed to adequately fit [18F]MNI-1038 data. [18F]MNI-1128 was best fitted with 2T model with low k_4.

Regional V_T of [18F]MNI-1126 in gray matter regions in rhesus (mean ± SD) was 30.2 ± 6.7 ml/cm^3 (animal M1) and 25.3 ± 5.8 ml/cm^3 (animal M2), with coefficients of variation (COV) of 22 % and 23 %, respectively. V_T was highest in the cerebrocortical areas, followed closely by the putamen and other striatal regions, lower in the midbrain and pons,
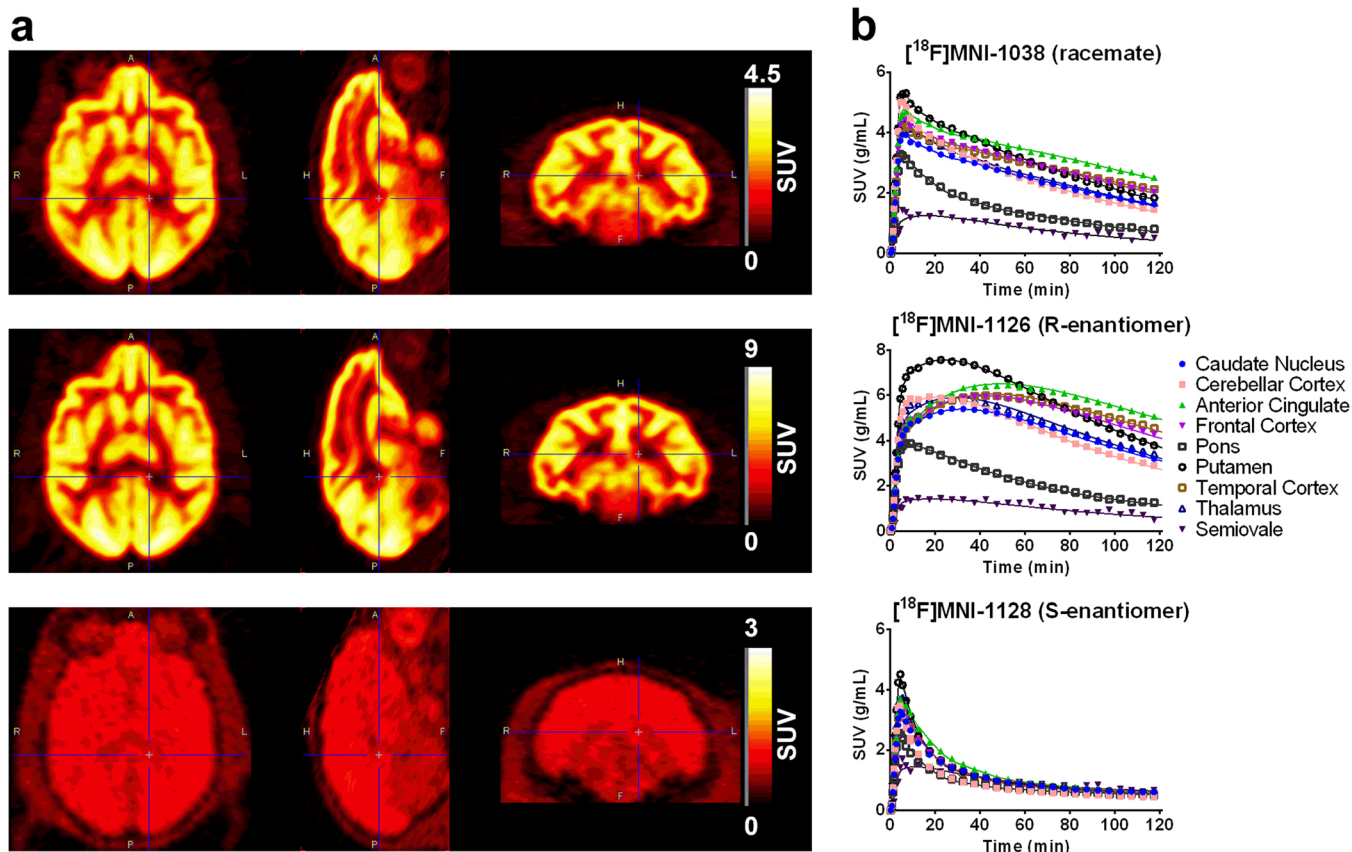

Fig. 4. **a** Average images (SUV 30–120 min p.i.) comparing the racemate [18F]MNI-1038 and the two enantiomers [18F]MNI-1126 (R-enantiomer) and [18F]MNI-1128 (S-enantiomer) in the same rhesus. Images were approximately scaled up to their SUV$_{max}$. **b** Time–activity curves (normalized to SUV) comparing the racemate [18F]MNI-1038 and the two enantiomers [18F]MNI-1126 (R-enantiomer)) and [18F]MNI-1128 (S-enantiomer) in the same rhesus. The continuous lines represent 2T ([18F]MNI-1038, [18F]MNI-1128), or 1T ([18F]MNI-1126) compartmental model curves.

and significantly lower in the centrum semiovale (Table 1). [^{18}F]MNI-1038 yielded V_T values of 17.7 ± 3.7 ml/cm^3 (M1) and COV = 21 %. BP$_{ND}$ of [^{18}F]MNI-1126 in gray matter regions in rhesus averaged to 4.7 ± 1.2 (M1) and 3.2 ± 1.0 (M2), with COV of 27–30 %. BP$_{ND}$ of [^{18}F]MNI-1038 was 3.0 ± 0.8 (M1). All regional V_T and BP$_{ND}$ values in rhesus at baseline and LEV pre-blocking are summarized in Table 1.

Across methods, regional V_T computed with compartmental modeling was highly correlated ($R^2 \sim 0.998$, slope ~ 1.0) with that from linear analysis methods (LGA and MA1). The tissue influx parameter of [^{18}F]MNI-1126, K_1, which is a measure of blood flow and tracer extraction was 0.68 ± 0.11 ml/cm^3/min in cortical regions and 0.2 ml/cm^3/min in the semiovale for rhesus M1, and 0.38 ± 0.09 ml/cm^3/min in cortical regions and 0.18 ml/cm^3/min in the semiovale for rhesus M2.

Both [^{18}F]MNI-1126 and [^{18}F]MNI-1038 were shown to be specific for SV2A by pre-blocking studies with LEV, which reduced the maximum uptake and the SUV peak times and increased the washout in a dose-dependent fashion, with the high dose of 30 mg/kg generating fast washout with a very similar kinetics in all regions (Fig. 5). LEV produced global occupancies of 86 % (cynomolgus), 81 % (rhesus) at 30 mg/kg, and 65 % (rhesus) at 10 mg/kg (Fig. 6). The V_T of the centrum semiovale at baseline ($V_T = 5.35$) and post blocking with the highest LEV dose of 30 mg/kg ($V_T = 4.48$) were comparable both between them and with V_{ND} estimated from the occupancy plot ($V_{ND} = 3.88$, 95 % CI = [2.65, 5.02]), which indicates that the centrum semiovale could be used as reference region to calculate BP$_{ND}$.

[^{18}F]MNI-1038 Dosimetry

Elimination of [^{18}F]MNI-1038 was exhibited *via* both urinary and hepatobiliary pathways. Organs with higher [^{18}F]MNI-1038 uptake included the urinary bladder, intestine, liver, brain, kidneys, and gall bladder. The limiting organ, which received the largest of $1.62E-01 \pm 8.70E-02$ mSv/MBq was the UB wall. The average effective dose (ED, ICRP-103) was between $2.16E-02$ and $2.31E-02$ mSv/MBq. Additional whole-body data, including [^{18}F]MNI-1038 whole-body images, organ kinetic values, organ absorbed doses, and whole-body effective doses, are presented in ESM.

Discussion

In an effort to find a fluorine-18 radiotracer for SV2A, we have screened several F-18 analogues of established SV2A radiotracer [^{18}F]UCB-J and then further characterized the lead compound in the racemic ([^{18}F]MNI-1038), *R*-enantiomer ([^{18}F]MNI-1126), and *S*-enantiomer ([^{18}F]MNI-1128) forms by performing a series of *in vivo* PET scans in
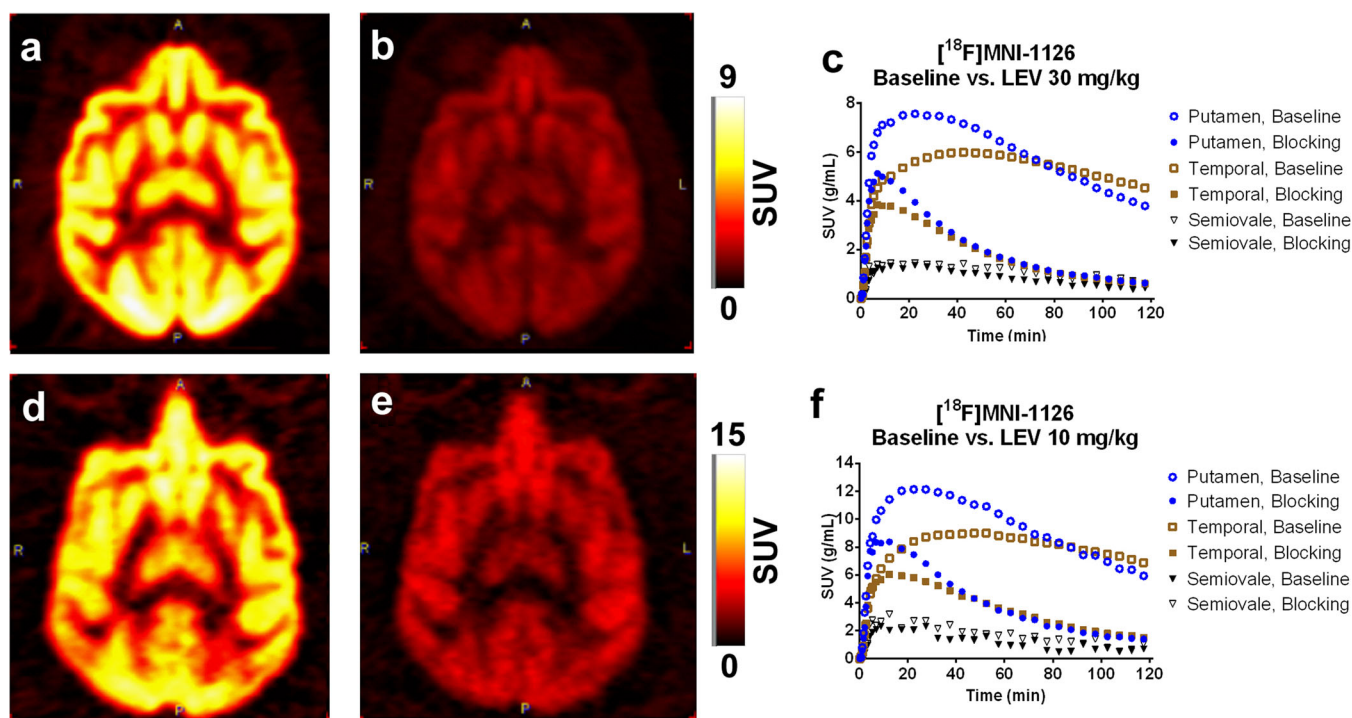

Fig. 5. [^{18}F]MNI-1126 SUV images averaged 30–120 min p.i. acquired in two different monkeys at baseline (**a**, **d**) and post blocking with 30 mg/kg (**b**) and 10.0 mg/kg (**e**) of levetiracetam (LEV). Plots on the right-hand side (**c**, **f**) show a comparison between TACs in the putamen, temporal cortex, and centrum semiovale from [^{18}F]MNI-1126 at baseline pre-blocking with LEV at 30 mg/kg (**c**) and 10 mg/kg (**f**).
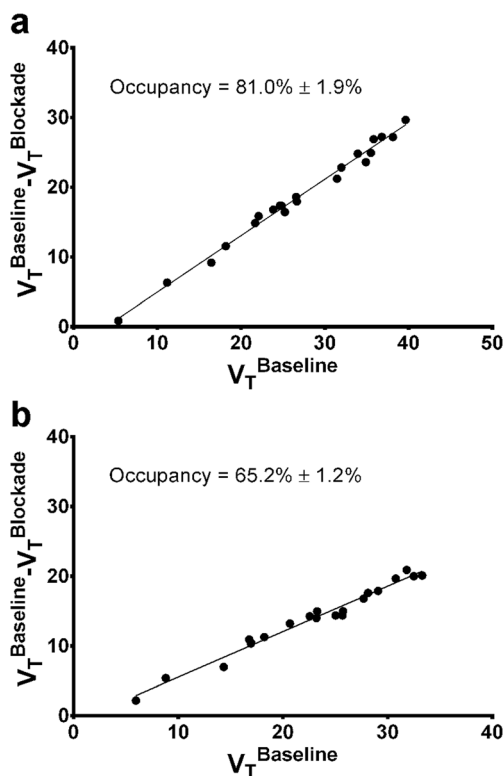
Fig. 6. Lassen occupancy plots generated from blocking studies with **a** 30 mg/kg and **b** 10.0 mg/kg of levetiracetam.

Table 1. Regional volumes of distribution, V_T, and binding potentials, BP_{ND}, (reference: centrum semiovale) of [18F]MNI-1038 and [18F]MNI-1126 at baseline and after pre-blocking with LEV. Monkeys are identified as M1 and M2

Region	V_T												BP_{ND}					
	[18F]MNI-1126[a]				[18F]MNI-1038[b]				[18F]MNI-1126				[18F]MNI-1038	
	M1		M2		M1				M1		M2		M1	
	Baseline	LEV, 30 mg/kg	Baseline	LEV, 10 mg/kg	Baseline	LEV, 30 mg/kg			Baseline	LEV, 30 mg/kg	Baseline	LEV, 10 mg/kg	Baseline	LEV, 30 mg/kg
Frontal lobe	31.98	9.15	29.08	12.42	18.84	6.28			4.98	1.04	3.88	1.98	3.26	0.56
Temporal lobe	33.94	9.13	28.12	11.67	19.53	5.82			5.35	1.04	3.72	1.81	3.42	0.45
Hippocampus	24.85	7.52	20.66	8.27	14.65	5.21			3.65	0.68	2.47	0.99	2.32	0.29
Amygdala	26.65	8.70	23.19	10.20	15.88	5.84			3.99	0.94	2.89	1.45	2.59	0.45
Parietal lobe	36.80	9.57	27.70	12.12	20.41	5.93			5.88	1.13	3.65	1.91	3.62	0.47
Occipital lobe	35.83	8.93	30.77	12.35	20.07	5.46			5.70	0.99	4.16	1.97	3.54	0.36
Anterior cingulate	38.13	10.92	33.30	14.67	23.24	6.61			6.13	1.44	4.59	2.53	4.26	0.64
Posterior cingulate	39.64	9.97	31.82	12.12	22.74	6.39			6.41	1.22	4.34	1.91	4.15	0.59
Insula	35.50	10.56	32.50	13.83	20.93	6.58			5.64	1.36	4.45	2.33	3.74	0.63
Caudate nucleus	25.23	8.81	25.03	11.80	15.18	6.48			3.72	0.97	3.20	1.84	2.44	0.61
Putamen	31.45	10.23	25.68	12.47	17.96	6.68			4.88	1.28	3.31	2.00	3.07	0.66
Ventral striatum	34.90	11.30	25.73	11.90	20.23	6.89			5.53	1.52	3.32	1.86	3.58	0.71
Globus pallidus	16.45	7.28	14.34	8.18	10.21	5.80			2.08	0.62	1.41	0.97	1.31	0.44
Thalamus	26.57	7.96	16.95	7.30	15.72	6.22			3.97	0.78	1.84	0.76	2.56	0.55
Hypothalamus	22.09	6.23	16.78	6.46	13.23	5.11			3.13	0.39	1.81	0.55	1.99	0.27
Cerebellar Cortex	23.84	7.05	22.56	9.23	14.42	5.54			3.46	0.57	2.78	1.22	2.26	0.38
Vermis	24.64	7.29	23.27	9.24	14.24	4.60			3.61	0.63	2.90	1.22	2.22	0.14
Cerebellar WM	18.17	6.63	16.96	7.25	11.82	4.52			2.40	0.48	1.84	0.74	1.68	0.12
Midbrain	21.68	6.82	18.22	7.71	12.30	5.64			3.06	0.52	2.06	0.85	1.78	0.40
Pons	11.17	4.87	8.81	3.74	7.90	4.23			1.09	0.09	0.48	−0.10	0.79	0.05
Semiovale	5.35	4.48	5.96	4.16	4.42	4.03								

[a]V_T from 1T model, [b]V_T from 2T model

cynomolgus and rhesus primates. In rhesus, [18F]MNI-1126 showed excellent brain uptake, with ubiquitous brain distribution characteristics to SV2A, and closely resembling UCB-J. Both [18F]MNI-1038 and [18F]MNI-1126 showed V_T highly correlated with UCB-J ($r > 0.99$) as reported in the literature [16].

The centrum semiovale, the region with lowest V_T, was used as a reference region to calculate BP_{ND}, based on reported evidence (19) from both *in vivo* and *in vitro* studies. BP_{ND} values with respect to the centrum semiovale of [18F]MNI-1126 were obtained as far as ~ 30 to 40 % higher than those reported for [11C]UCB-J. However, this result could be attributed in part to differences between primates considering the limited number of animals used in the study, as well as to how centrum semiovale region was defined and delineated on the brain images. Ideally, one would expect the V_T of the centrum semiovale to closely approximate the V_{ND} obtained from occupancy plots. However, most likely due to resolution and spillover effects, and in absence of partial volume correction, we found a semiovale V_T slightly larger than V_{ND}.

The specificity for SV2A was assessed *via* blocking with levetiracetam at two dose levels. Administration of LEV at high dose (30 mg/kg) produced 80–85 % occupancy as measured by both [18F]MNI-1126 and [18F]MNI-1038 in two primate species, similar to values reported with [11C]UCB-J at the same dose level. SV2A occupancy was also shown to be dose dependent. The occupancy was robust across all cortical regions. To assess the impact of using the centrum semiovale on occupancy measurements, average regional occupancy computed using BP_{ND} with respect to semiovale at baseline and blocking was compared to the global occupancy. Differences between the two measures were within 3 %, indicating that using the centrum semiovale as reference, even without partial volume correction, is appropriate in occupancy studies.

The radiation exposure to [18F]MNI-1038 as estimated from the whole-body imaging studies that were conducted was estimated to be 22.3 μSv/MBq on average, which is the equivalent of 4.13 mSv per 185 MBq (5 mCi) injection. This figure is in line with other F-18-labeled tracers in routine use (*e.g.*, 19 μSv/MBq for 2-deoxy-[18F]fluoro-D-glucose) and would allow several scans to be performed in the same subject with a 185-MBq dose. The limiting organ, UB wall, limits the number of 185-MBq injections to 5 per year according to 21 CFR 361.1. The biodistribution and dosimetry of [18F]MNI-1126, which is the active enantiomer of [18F]MNI-1038, is expected to be very similar since SV2A is primarily present in the brain and spinal cord.

Conclusions

We have reported the development and the evaluation of 18F-labeled tracers for imaging SV2A proteins. The best candidate, [18F]MNI-1126 presented excellent *in vivo* binding properties as demonstrated by preliminary studies in non-human primates.

[18F]MNI-1126 had regional brain uptake consistent with SV2A protein distribution and presented similar or improved specific binding measures compared with currently available SV2A PET tracers. The dosimetry of [18F]MNI-1038 (racemate) easily met the criteria for radiation exposure in human clinical studies. Based on the initial *in vivo* preclinical evaluation presented, [18F]MNI-1126 demonstrated excellent qualities as a F-18-labeled PET tracer for use in multicenter SV2A imaging trials. First human clinical studies are currently ongoing with [18F]MNI-1126.

Conflict of Interest

References

1. Bajjalieh SM, Scheller RH (1995) The biochemistry of neurotransmitter secretion. J Biol Chem 270:1971–1974
2. Bajjalieh SM, Peterson K, Linial M, Scheller RH (1993) Brain contains two forms of synaptic vesicle protein 2. Proc Natl Acad Sci U S A 90:2150–2154
3. Douaud M, Feve K, Pituello F, Gourichon D, Boitard S, Leguern E, Coquerelle G, Vieaud A, Batini C, Naquet R, Vignal A, Tixier-Boichard M, Pitel F (2011) Epilepsy caused by an abnormal alternative splicing with dosage effect of the SV2A gene in a chicken model. PLoS One 6:e26932
4. Kaminski RM, Matagne A, Leclercq K, Gillard M, Michel P, Kenda B, Talaga P, Klitgaard H (2008) SV2A protein is a broad-spectrum anticonvulsant target: functional correlation between protein binding and seizure protection in models of both partial and generalized epilepsy. Neuropharmacology 54:715–720
5. Kaminski RM, Gillard M, Klitgaard H (2012) Targeting SV2A for discovery of antiepileptic drugs. In: Jasper's basic mechanisms of the epilepsies [Internet]. 4th edition. Bethesda (MD): National Center for Biotechnology Information (US)
6. Nicolas JM, Hannestad J, Holden D, Kervyn S, Nabulsi N, Tytgat D, Huang Y, Chanteux H, Staelens L, Matagne A, Mathy FX, Mercier J, Stockis A, Carson RE, Klitgaard H (2016) Brivaracetam, a selective high-affinity synaptic vesicle protein 2A (SV2A) ligand with preclinical evidence of high brain permeability and fast onset of action. Epilepsia 57:201–209
7. Matagne A, Margineanu DG, Kenda B, Michel P, Klitgaard H (2008) Anti-convulsive and anti-epileptic properties of brivaracetam (ucb 34714), a high-affinity ligand for the synaptic vesicle protein, SV2A. Br J Pharmacol 154:1662–1671
8. Stockburger C, Miano D, Baeumlisberger M, Pallas T, Arrey TN, Karas M, Friedland K, Müller WE (2016) A mitochondrial role of SV2a protein in aging and Alzheimer's disease: studies with levetiracetam. J Alzheimers Dis 50:201–215
9. Finnema SJ, Nabulsi NB, Eid T et al (2016) Imaging synaptic density in the living human brain. Sci Transl Med 8:348ra96
10. Preshlock S, Tredwell M, Gouverneur V (2016) 18F-labeling of arenes and heteroarenes for applications in positron emission tomography. Chem Rev 116:719–766
11. Mercier J, Provins L, Valade A (2017) Discovery and development of SV2A PET tracers: potential for imaging synaptic density and clinical applications. Drug Discov Today Technol 25:45–52

12. Becker G, Warnier C, Serrano ME, Bahri MA, Mercier J, Lemaire C, Salmon E, Luxen A, Plenevaux A (2017) Pharmacokinetic characterization of [^{18}F]UCB-H PET radiopharmaceutical in the rat brain. Mol Pharm 14:2719–2725

13. Bahri MA, Plenevaux A, Aerts J, Bastin C, Becker G, Mercier J, Valade A, Buchanan T, Mestdagh N, Ledoux D, Seret A, Luxen A, Salmon E (2017) Measuring brain synaptic vesicle protein 2A with positron emission tomography and [^{18}F]UCB-H. Alzheimers Dement (N Y) 3:481–486

14. Warnier C, Lemaire C, Becker G, Zaragoza G, Giacomelli F, Aerts J, Otabashi M, Bahri MA, Mercier J, Plenevaux A, Luxen A (2016) Enabling efficient positron emission tomography (PET) imaging of synaptic vesicle glycoprotein 2A (SV2A) with a robust and one-step radiosynthesis of a highly potent ^{18}F-labeled ligand ([(18)F]UCB-H). J Med Chem 59:8955–8966

15. Finnema SJ, Nabulsi NB, Mercier J, et al. (2017) Kinetic evaluation and test-retest reproducibility of [11C]UCB-J, a novel radioligand for positron emission tomography imaging of synaptic vesicle glycoprotein 2A in humans. J Cereb Blood Flow Metab 271678X17724947

16. Nabulsi NB, Mercier J, Holden D, Carre S, Najafzadeh S, Vandergeten MC, Lin SF, Deo A, Price N, Wood M, Lara-Jaime T, Montel F, Laruelle M, Carson RE, Hannestad J, Huang Y (2016) Synthesis and preclinical evaluation of 11C-UCB-J as a PET tracer for imaging the synaptic vesicle glycoprotein 2A in the brain. J Nucl Med 57:777–784

17. Rohlfing T, Kroenke CD, Sullivan EV et al (2012) The INIA19 template and NeuroMaps atlas for primate brain image parcellation and spatial normalization. Front Neuroinform 6:27

18. Ballanger B, Tremblay L, Sgambato-Faure V, Beaudoin-Gobert M, Lavenne F, le Bars D, Costes N (2013) A multi-atlas based method for automated anatomical Macaca fascicularis brain MRI segmentation and PET kinetic extraction. Neuroimage 77:26–43

19. Logan J, Fowler JS, Volkow ND, Wolf AP, Dewey SL, Schlyer DJ, MacGregor RR, Hitzemann R, Bendriem B, Gatley SJ, Christman DR (1990) Graphical analysis of reversible radioligand binding from time-activity measurements applied to [N-^{11}C-methyl]-(-)-cocaine PET studies in human subjects. J Cereb Blood Flow Metab 10:740–747

20. Ichise M, Toyama H, Innis RB, Carson RE (2002) Strategies to improve neuroreceptor parameter estimation by linear regression analysis. J Cereb Blood Flow Metab 22:1271–1281

21. Cunningham VJ, Rabiner EA, Slifstein M, Laruelle M, Gunn RN (2010) Measuring drug occupancy in the absence of a reference region: the Lassen plot re-visited. J Cereb Blood Flow Metab 30:46–50

22. (2006) Human alimentary tract model for radiological protection. ICRP Publication 100. A report of The International Commission on Radiological Protection. Ann ICRP 36:25–327, iii

23. Ziessman HA, Jones DA, Muenz LR, Agarval AK (2003) Cholecystokinin cholescintigraphy: methodology and normal values using a lactose-free fatty-meal food supplement. J Nucl Med 44:1263–1266

24. Thomas SR, Stabin MG, Chen CT, Samaratunga RC (1999) MIRD Pamphlet No. 14 revised: a dynamic urinary bladder model for radiation dose calculations. Task Group of the MIRD Committee, Society of Nuclear Medicine. J Nucl Med 40:102S–123S

25. Stabin MG, Sparks RB, Crowe E (2005) OLINDA/EXM: the second-generation personal computer software for internal dose assessment in nuclear medicine. J Nucl Med 46:1023–1027

26. (2002) Basic anatomical and physiological data for use in radiological protection: reference values. A report of age- and gender-related differences in the anatomical and physiological characteristics of reference individuals. ICRP Publication 89. Ann ICRP 32:5–265

27. (2007) The 2007 Recommendations of the International Commission on Radiological Protection. ICRP publication 103. Ann ICRP 37:1–332

28. (1991) ICRP, 1991. 1990 Recommendations of the International Commission on Radiological Protection. ICRP Publication 60. Ann ICRP 21

29. Makaravage KJ, Brooks AF, Mossine AV, Sanford MS, Scott PJH (2016) Copper-mediated radiofluorination of arylstannanes with [^{18}F]KF. Org Lett 18:5440–5443

30. Mossine AV, Brooks AF, Makaravage KJ (2015) Synthesis of [^{18}F]arenes via the copper-mediated [18F]fluorination of boronic acids. Org Lett 17:5780–5783